

Learning Hamiltonians for solid-state quantum simulators

Jarosław Pawłowski^{✉*} and Mateusz Krawczyk[✉]

*Institute of Theoretical Physics, Wrocław University of Science and Technology,
Wybrzeże Wyspiańskiego 27, 50-370 Wrocław, Poland*

We introduce a generalizable framework for learning to identify effective Hamiltonians directly from experimental data in solid-state quantum systems. Our approach is based on a physics-informed neural network architecture that embeds physical constraints directly into the model structure. Unlike purely data-driven supervised schemes, the proposed unsupervised autoencoder-based method incorporates the governing physics (here, the S-matrix formalism) within the decoder network, ensuring that the learned representations remain physically meaningful. Through numerical learning experiments, we demonstrate automated characterization of programmable solid-state simulators from transport measurements, exemplified by a triple quantum dot chain. The trained model generalizes beyond the training domain and accurately infers Hamiltonian parameters from transport data. While the model has finite capacity—leading to degraded performance when the parameter space becomes excessively large or structurally diverse—we identify regimes in which robust generalization is maintained. We further show how to train the model to handle noisy measurements, reflecting realistic experimental conditions.

Introduction.—Machine learning (ML) techniques have been widely explored in solid-state physics, including phase identification [1–4] and materials discovery through the prediction of chemical and electronic properties [5–8]. A central challenge in this area is the extraction of effective Hamiltonians \mathcal{H} from experimental or simulated observables [9]. Existing approaches broadly fall into two categories: optimization-based inverse methods, such as evolutionary algorithms and heuristic searches [10–13], and supervised learning schemes [14–19], which often struggle with robustness and generalization.

Hamiltonian learning (HL) has shown particular promise in nanoscale solid-state platforms, including the identification of quantum nanomagnets from spectral data [14, 15], classification of skyrmionic magnetic textures [16], and ML-assisted control and readout of molecular spin qubits [20]. Beyond transport measurements, HL has also been applied to density-of-states data for automated band-structure inference [21] and to the analysis of local patterns in moiré materials [22, 23]. Learning tight-binding Hamiltonians is likewise emerging as an important research direction [24, 25]. Finally, learning Hamiltonian dynamics constitutes another active line of research, with applications ranging from classical systems [26, 27] and generic quantum dynamics [28, 29] to superconducting quantum processors [30].

Gate-defined quantum dots (QDs) hosting single electrons or holes are promising platforms for solid-state quantum computing due to their electrical tunability and scalability, and have recently attracted interest as programmable quantum simulators [31–33]. In particular, minimal realizations of the Kitaev chain in QD arrays—based on elastic cotunneling and crossed Andreev reflection and supporting so-called *poor man’s* Majorana zero modes (MZMs) [34]—have attracted significant attention [35, 36]. Rashba quantum dot chains have also

been proposed as alternative simulator platforms capable of hosting MZMs [37, 38].

At the same time, ML-assisted autotuning of QD-based quantum simulators using transport measurements is gaining increasing interest [10, 39–42]. The use of transport measurements in the form of *conductance maps* [33, 43] to extract information about the system Hamiltonian [9, 13, 17, 18, 44–46] appears to be a promising route toward automated parameter tuning. In particular, inverting measured conductance matrices to determine electrostatic potential disorder—using evolutionary optimization [13], supervised neural networks [45–47], or hybrid approaches [48]—provides a natural starting point for precise inference of \mathcal{H} parameters relevant to MZMs.

Physical constraints can be incorporated into neural network (NN) models in two principal ways: by enforcing symmetry-respecting representations (geometric deep learning [49]) or by constraining solutions to satisfy governing differential equations, as in physics-informed neural networks (PINNs) [50–52]. Both approaches typically rely on supervised training, which can be limiting in realistic HL scenarios where the parameters of effective Hamiltonians are not directly accessible. Here, we adopt a physics-decoder (PD) architecture [53–56], shown in Fig. 1(b), inspired by PINNs but formulated as a fully unsupervised autoencoder-based framework. In this scheme, the encoder infers Hamiltonian parameters, while the decoder explicitly implements the underlying physics for the assumed Hamiltonian family—a strategy that can be readily generalized beyond the present setting. HL with physics-informed training schemes remains relatively underexplored and constitutes an active area of research [24, 25, 57, 58].

Quantum dots chain.—To demonstrate the working principle of the method, we define a simple simulator consisting of a chain of $N = 3$ QDs, yet sufficiently complex to illustrate the robustness of the approach. We consider

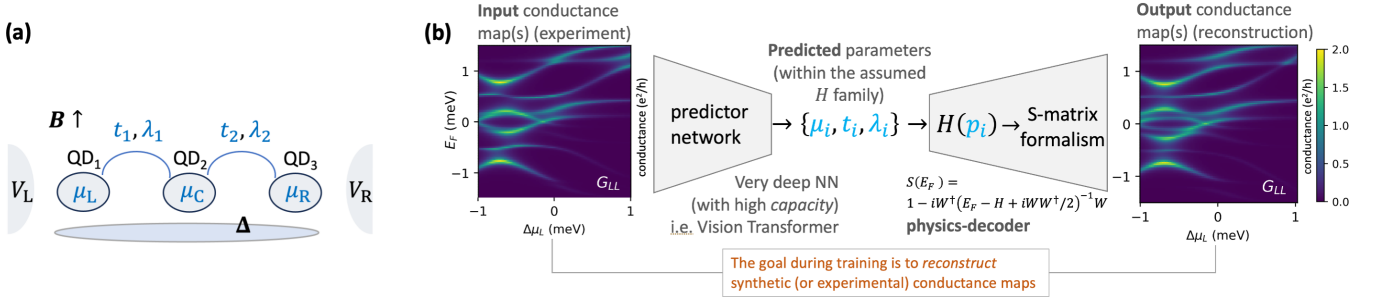


FIG. 1. (a) Chain of the Rashba QDs. (b) Proposed HL architecture composed of encoder—predictor and physics-decoder.

a \mathcal{H} family that defines the Kitaev-chain simulator based on a Rashba QD chain coupled with a nearby s -wave superconductor [37], depicted in Fig. 1(a). The Hamiltonian describing chain of spinful single-level QDs with local potential μ_n , Zeeman energy V_Z , proximity-induced superconducting (s -wave) pairing Δ_n , and Rashba spin-orbit vector λ_n , which modifies the inter-dot hopping t_n , is defined as:

$$\begin{aligned}
 H^{\text{QDs}} = & \sum_{n,s,s'} \left[(-\mu_n \sigma_0 + V_Z \sigma_z)_{ss'} c_{n,s}^\dagger c_{n,s'} \right. \\
 & + \frac{1}{2} \left((\Delta_n i \sigma_y)_{ss'} c_{n,s}^\dagger c_{n,s'}^\dagger + \text{h.c.} \right) \\
 & \left. + (t_n (e^{i\lambda_n \cdot \sigma})_{ss'} c_{n,s}^\dagger c_{n+1,s'} + \text{h.c.}) \right], \quad (1)
 \end{aligned}$$

where σ_i are Pauli matrices in spin space (indexed by s and s'), and n numbers QDs in the chain. For simplicity we assume uniform pairing $\Delta_n = 0.25$ meV, the Rashba vector in a form $\lambda_n = \lambda_n [0, 1, 0]$, and the global Zeeman field $V_Z = 0.5$ meV. The rest control parameters, i.e., $\{\mu_n, t_n, \lambda_n\} \equiv P$ (7 in total for $N = 3$ QDs chain) can be tuned electrically (via local gating). One set (yet uniform) of parameters includes: $\mu_n = 0.6$ meV, $t_n = 0.25$ meV, $\lambda_n = 0.27\pi$ we call *reference parameters*, P_0 . They define so-called *sweet spot* leading to MZMs emergence, discussed in detail in Supplementary Material (SM). The configuration of eigenstates for $N = 7$ and $N = 3$ is shown in Fig. 2(a) and Figs. 2(b,c) respectively. The Rashba length $\lambda_n = 0.27\pi$ was tuned so that at $\mu = 0.6$ meV two energy levels touch at zero energy (c.f. Fig. 2(b,c)).

Transport measurements.—The analyzed system can be characterized via transport measurements. The conductance G through the QD chain is calculated using the S -matrix formalism in the wide-band limit [43] via the Weidenmüller formula [59, 60] for QDs coupled to normal leads:

$$S[H](E_F) = \mathbf{1} - iW^\dagger(E_F - H + \frac{i}{2}WW^\dagger)^{-1}W, \quad (2)$$

with the tunneling matrix defined as $W = \text{diag}(1, 0, 1) \otimes \text{diag}(\sqrt{\Gamma}, \sqrt{\Gamma}, -\sqrt{\Gamma}, -\sqrt{\Gamma})$ and the dot-lead coupling $\Gamma = 0.1$ meV. If we reshape the S -matrix accordingly: $S =$

$S_{n,p,s,n',p',s'}$ ($n = L, C, R$ indexing dots, $p = 1, 2$ particle, and s —spin subspaces), then the respective reflection matrices: $s_{s,s}^{ee}(i, j) = S_{i,1,s,j,1,s'}$ and $s_{s,s}^{he}(i, j) = S_{i,2,s,j,1,s'}$ give differential conductance as,

$$\begin{aligned}
 G[S(E_F)]_{ij} = & \frac{dI_i}{dV_j} = 2\delta_{ij} - \text{tr}(s^{ee}(i, j)s^{ee}(i, j)^\dagger) \\
 & + \text{tr}(s^{he}(i, j)s^{he}(i, j)^\dagger) \quad (3)
 \end{aligned}$$

in unit of e^2/h , $i, j = L, R$ denoting left (L) or right (R) lead—see Fig. 1(a), and E_F being the Fermi energy in the leads. Note that the same formula is implemented in the PD shown in Fig. 1(b). The input maps include 4 conductance G_{ij} components: G_{LL} , G_{LR} , G_{RL} , and G_{RR} , where for instance $G_{LL} = \frac{dI_L}{dV_L}$, with I_L denoting current through the left lead, and V_L is the bias voltage of the left lead. Similarly, other components can be defined by using different combinations of the leads. Notably, each conductance map is defined by 100×100 2D plot of G_{ij} as a function of some parameter and E_F . We utilize 4 maps per each component $G(E_f, \Delta l)$: 3 for $l = \mu_{n=L,C,R}$ variation (with respect to actual parameter P) and 1 for $l = V_Z$ variation: 16 maps in total serving as the input. Figs. 2(d-f) shows the conductance maps (G_{LL} component) for the reference parameters P_0 , highlighting the emerged zero-bias peak (orange arrow).

Neural architecture and training.—The proposed method uses the conductance maps tensor G as a high-dimensional visual input for the predictor NN (encoder), as well as to define the physics-inspired decoder—PD (teacher network) for unsupervised training. The model architecture is presented in Fig. 1(b). It is of autoencoder-form with predictor NN coupled to PD network through parameters P latent space, and can be denoted as

$$\hat{G} = \text{PD}(\text{NN}(G) = P), \quad \text{PD}(P) \equiv G[S[\mathcal{H}(P)]]. \quad (4)$$

The encoder analyzes the G maps and predicts the parameter vector P ; PD explicitly implements the transport physics using Eqs. 2 and 3, with the assumed systems family $\mathcal{H} = H^{\text{QDs}}$, defined in Eq. 1. The objective is for the reconstructed map \hat{G} (the PD output) to

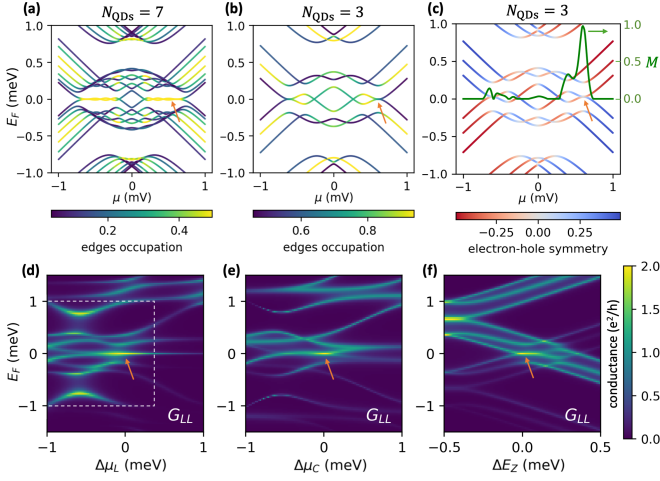


FIG. 2. Rashba chain of QDs proximitized by an s -wave superconductor. Top row: eigenstates as a function of voltage offset with colors encoding: (a,b) edges (L and R dot) occupation, (c) electron-hole symmetry. Reference parameters configuration P_0 , giving MZM-like states, is marked by orange arrow. Bottom row: conductance maps as a function of (d) voltage applied to the left dot, (e) voltage on the center dot, and (f) the Zeeman field.

match the (encoder) input G —by minimizing loss function $\mathcal{L}(G, \hat{G}) = \|G - \hat{G}\|^2$. We adapt a pretrained vision transformer (ViT) architecture [61] (patch size 16×16 , 12 heads, 12 layers, $\sim 86\text{M}$ parameters) with input layers adjusted to process 16-channel ($16 \times 100 \times 100$) input tensor G and returning vector of the Hamiltonian parameters P . Training (\mathcal{L} minimization) is performed for 300 epochs (with a properly tuned learning-rate scheduler) using 10-50k data points ($G(P_{\text{in}})$ maps) for parameter vectors P_{in} sampled from different regions of the parameter space, as described in the Results section.

Results.—To demonstrate the validity of the PD concept, we performed HL of $\mathcal{H} = H^{\text{QDs}}$ parameters, i.e. $P = \{\mu_L, \mu_C, \mu_R, t_1, t_2, \lambda_1, \lambda_2\}$ for the triple-QD Rashba chain, as described above. After the training using synthetic $G(P_{\text{in}})$ maps with P_{in} sampled from training sets denoted as white boxes in Figs. 3-6, the predictor NN can predict the (learned) Hamiltonian parameters P for a given G . Sampling Δl in the range $[a, b]$ means that parameter $l \in [a, b] + P_0$, e.g., all μ_n were sampled from some $[\mu_a, \mu_b] + 0.6$ meV. The robustness of the predictor is shown in Fig. 3. The middle and bottom rows (d-g) show pairs of: input conductance maps (middle), and conductance maps *reconstructed* (calculated) using the predicted parameters (bottom). The better the parameter prediction, the closer the maps in each pair. The pairs presented are for different parameter configurations, indicated by the respective symbols in the top row (a-c). In the top row the reconstruction error $\langle |G - \hat{G}| \rangle$ is presented as a function of various parameters variation ($\Delta l_1, \Delta l_2$) giving three different cuts in the parameter P space. Re-

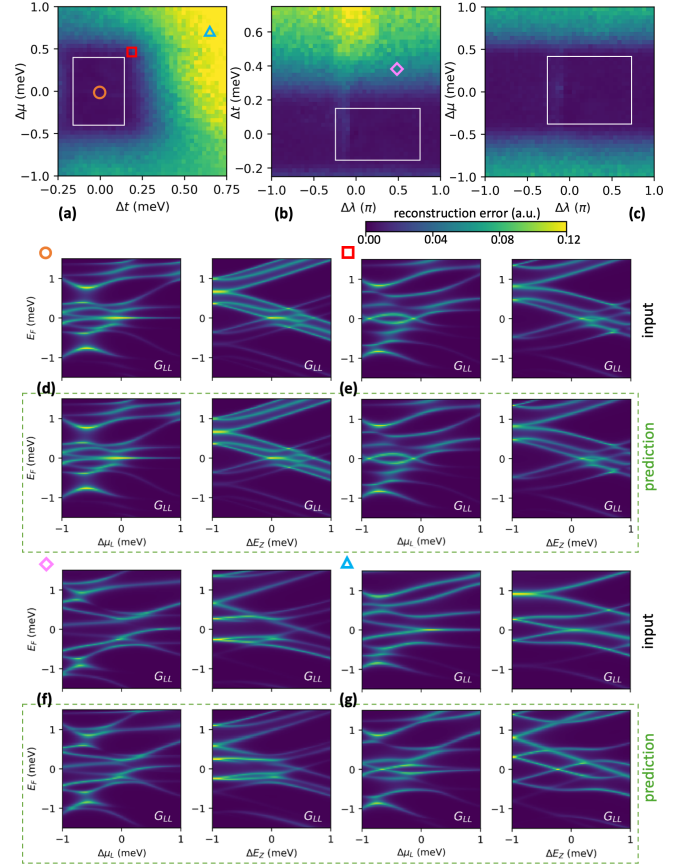


FIG. 3. Results for the HL of the Rashba chain, Eq. 1, of three quantum dots proximitized by an s -wave superconductor. Top row (a-c): error for the conductance maps reconstruction (via the predicted parameters) as a function of parameter variations—the white box denotes the region where training data was sampled. Middle (d,e) and bottom (f,g) rows: example input and predicted conductance maps (shown as middle/bottom pairs) for various parameter configurations indicated by the respective symbols. The default configuration that yields MZMs is marked with an orange circle

construction error is averaged over all channels and pixels on G_{ij} maps, and over variations of different parameters of a given category (e.g., $\Delta\mu$ means all variations of potentials $\Delta\mu_n$).

Inspection of the G_{LL} maps in Fig. 3 for parameters (d) within the training set (denoted by an orange circle on (a), corresponding to P_0), or (e) close to it (red square) shows that the reconstructed maps match the input maps almost perfectly. Moving slightly further away (f, pink diamond), small reconstruction errors begin to appear, although the overall structure of the conductance bands remains qualitatively well reproduced. However, when we move farther from the training set (g, blue triangle), the resulting structure of the conductance peaks in the G maps becomes noticeably different. These results demonstrate that the PD architecture is capable of learning the complex structure of the conductance features that arise

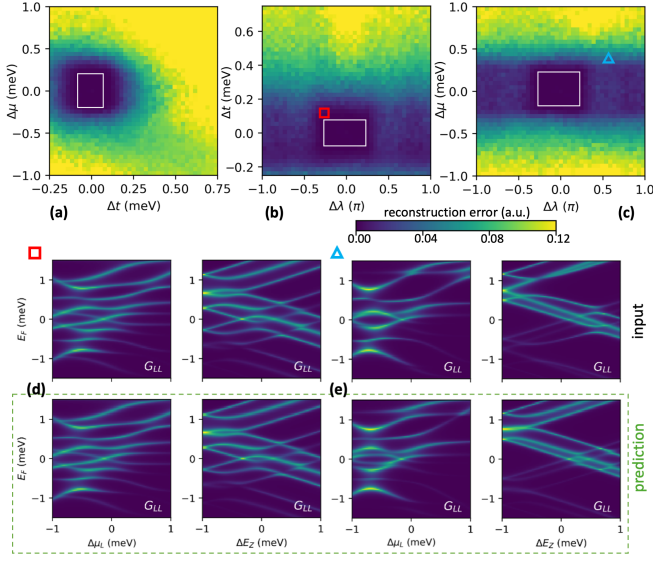


FIG. 4. HL results for a smaller training range, denoted by white boxes on the conductance reconstruction error maps (a-c) within the parameter space. Two specific G reconstruction cases (d,e) are indicated in the parameter space by a red square in (b) and a blue triangle in (c), respectively.

even in this simple triple-QD system. More importantly, the model provides accurate predictions for regions of parameter space outside the training domain (outside the white rectangles in Fig. 3(a-c)). This indicates that the physics-informed PD architecture possesses a strong ability to generalize. Importantly, the sampling of the 7-dimensional training space is relatively sparse: 10k samples correspond to approximately $(10^4)^{\frac{1}{7}} \simeq 3.7$ points per dimension.

To better investigate this property, we evaluated the NN predictor performance for a smaller training region—indicated in Fig. 4, and for a larger one—shown in Fig. 5. As expected, the smaller training region (reduced by a factor of 2^3) leads to accurate parameter predictions only within a correspondingly smaller volume of the parameter space P . Nevertheless, even in this case there remains a region outside the training set where the model generalizes well. Moreover, the ratio of this generalization vol-

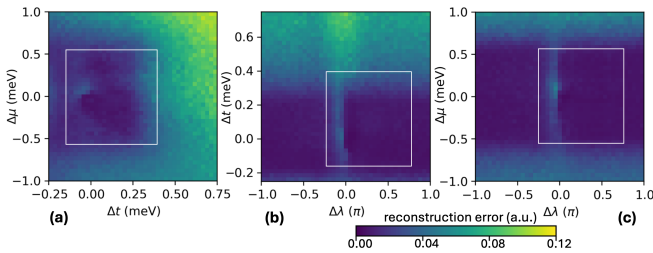


FIG. 5. HL results for a larger training range, indicated by wider white boxes on the conductance reconstruction error maps (a-c). In this case, 50k training samples were used.

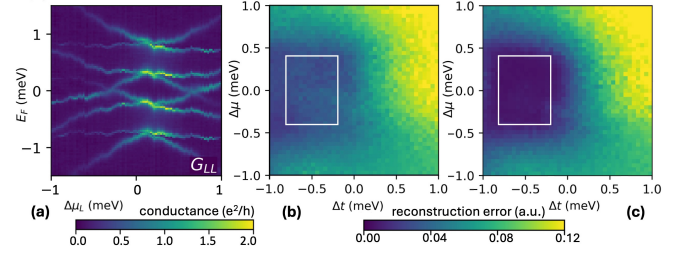


FIG. 6. HL from noisy data: (a) noisy conductance maps lead to (b) slightly degraded predictions. However, retraining the model with noisy samples included in the training data (c) restores the prediction performance.

ume to the training volume is slightly larger than in the configuration shown in Fig. 3. This can be attributed to the fact that, in the vicinity of the reference parameters P_0 (emergence of MZMs), the structure of peaks on the G map is relatively similar, making it easier for the NN to learn.

In the opposite extreme, presented in Fig. 5—we observe that for a larger training volume (increased by a factor of $1.5 \times 2 \times 1 = 3$) the model correctly predicts the parameters $\mathcal{H}(P)$ over nearly the entire explored parameter space P . Importantly, in this case we increased the number of training samples to 50k (in the previous configurations shown in Figs. 3 and 4, we used 10k samples). However, as a characteristic trade-off, the price of covering such a broad range of G -maps variability is a slightly reduced average accuracy of parameter predictions, even within the training region itself. This clearly indicates that we are approaching the NN capacity limit.

Resilience to noise.—In the proposed approach, we assume that the NN model is first trained on synthetically generated data and subsequently transferred to experimental measurement data. However, experimental data may exhibit characteristics different from those of the synthetic dataset; in particular, they may contain noise. To test this and emulate realistic experimental conditions, we augmented the synthetic conductance maps $G_{ij}(E_f, \Delta l)$ by including two different noise contributions, according to

$$\tilde{G}_{ij}(E_f, \Delta l) = G_{ij}^{\text{warp}}(E_f, \Delta l) + \delta G_{ij}^{\text{add}}(E_f, \Delta l), \quad (5)$$

where E_F is the Fermi energy in the leads and l denotes the detuned control parameter, corresponding either to the chemical potential of a selected quantum dot ($l = \mu_n$) or to the Zeeman field ($l = V_Z$). The term G_{ij}^{warp} describes distortions caused by charge noise and gate drift, while $\delta G_{ij}^{\text{add}}$ accounts for additive instrumental noise. Both are discussed in detail in SM.

We next examine the robustness of the proposed method to noise defined in this way—an example of a noisy conductance map \tilde{G} is shown in Fig. 6(a). When testing the model presented in Fig. 3 on such noisy maps,

the prediction quality naturally degrades—see Fig. 6(b). However, if the noise present in the experimental setup is well characterized, we can sample \tilde{G} and add to the training data (10k samples were added). In Fig. 6(c) we show the reconstruction error for the NN model trained on the augmented conductance map set. It is visible that the model is now capable of predicting the \mathcal{H} parameters even from the noisy conductance maps.

Note also that the PD architecture can be used for efficient GPU-parallelized synthetic data generation, as was done in this work for conductance map sets.

Summary.—In this Letter we present an architecture and training algorithms for deep neural networks capable of identifying (predicting or discovering—depending on the application context) the parameters of Hamiltonians in quantum systems, including quantum simulators based on nanostructures. This work focuses on quantum simulators described by lattice Hamiltonians implemented in chains of quantum dots (QDs), together with their basic characterization through transport measurements. Specifically, it addresses the reconstruction of the effective Hamiltonian of a gated QD chain from conductance maps as a function of the applied gate voltages. We propose a natural mechanism for enforcing the underlying physics within the learning procedure. Moreover, the proposed scheme for defining and training a physics-informed neural network model can be applied to other areas of physics—wherever the underlying equations can be embedded in the form of differentiable formulas.

ACKNOWLEDGMENTS

We gratefully acknowledge Polish high-performance computing infrastructure PLGrid (HPC Centers: ACK Cyfronet AGH) for providing computer facilities and support within computational grant no. PLG/2025/018433.

* jaroslaw.pawlowski@pwr.edu.pl

- [1] E. P. L. van Nieuwenburg, Y.-H. Liu, and S. D. Huber, Learning phase transitions by confusion, *Nature Physics* **13**, 435 (2017).
- [2] K. Ch'ng, J. Carrasquilla, R. G. Melko, and E. Khatami, Machine learning phases of strongly correlated fermions, *Phys. Rev. X* **7**, 031038 (2017).
- [3] P. Zhang, H. Shen, and H. Zhai, Machine learning topological invariants with neural networks, *Phys. Rev. Lett.* **120**, 066401 (2018).
- [4] Y. Mao, Q. He, and X. Zhao, Designing complex architected materials with generative adversarial networks, *Science Advances* **6**, eaaz4169 (2020), <https://www.science.org/doi/pdf/10.1126/sciadv.aaz4169>.
- [5] K. T. Schütt, H. E. Sauceda, P.-J. Kindermans, A. Tkatchenko, and K.-R. Müller, Schnet – a deep learning architecture for molecules and materials, *The Journal of Chemical Physics* **148**, 241722 (2018), <https://pubs.aip.org/aip/jcp/article-pdf/doi/10.1063/1.5019779/16655678/241722.1.online.pdf>.
- [6] A. Merchant, S. Batzner, S. S. Schoenholz, M. Aykol, G. Cheon, and E. D. Cubuk, Scaling deep learning for materials discovery, *Nature* **624**, 80 (2023).
- [7] A. K. Cheetham and R. Seshadri, Artificial intelligence driving materials discovery? perspective on the article: Scaling deep learning for materials discovery, *Chemistry of Materials* **36**, 3490 (2024).
- [8] J. Qi, T. W. Ko, B. C. Wood, T. A. Pham, and S. P. Ong, Robust training of machine learning interatomic potentials with dimensionality reduction and stratified sampling, *npj Computational Materials* **10**, 43 (2024).
- [9] V. Gebhart, R. Santagati, A. A. Gentile, E. M. Gauger, D. Craig, N. Ares, L. Banchi, F. Marquardt, L. Pezzè, and C. Bonato, Learning quantum systems, *Nature Reviews Physics* **5**, 141 (2023).
- [10] L. Lunczer, P. Leubner, M. Endres, V. L. Müller, C. Brüne, H. Buhmann, and L. W. Molenkamp, Approaching quantization in macroscopic quantum spin hall devices through gate training, *Phys. Rev. Lett.* **123**, 047701 (2019).
- [11] A. J. Lew, K. Jin, and M. J. Buehler, Designing architected materials for mechanical compression via simulation, deep learning, and experimentation, *npj Computational Materials* **9**, 80 (2023).
- [12] K. Inui and Y. Motome, Inverse Hamiltonian design of highly entangled quantum systems, *Phys. Rev. Res.* **6**, 033080 (2024).
- [13] M. Thamm and B. Rosenow, Conductance based machine learning of optimal gate voltages for disordered Majorana wires, *Phys. Rev. B* **109**, 045132 (2024).
- [14] G. Lupi and J. L. Lado, Hamiltonian-learning quantum magnets with nonlocal impurity tomography, *Phys. Rev. Appl.* **23**, 054077 (2025).
- [15] N. Karjalainen, Z. Lippo, G. Chen, R. Koch, A. O. Fumega, and J. L. Lado, Hamiltonian inference from dynamical excitations in confined quantum magnets, *Phys. Rev. Appl.* **20**, 024054 (2023).
- [16] D. Feng, Z. Guan, X. Wu, Y. Wu, and C. Song, Classification of skyrmionic textures and extraction of Hamiltonian parameters via machine learning, *Phys. Rev. Appl.* **21**, 034009 (2024).
- [17] R. Koch, D. van Driel, A. Bordin, J. L. Lado, and E. Greplova, Adversarial Hamiltonian learning of quantum dots in a minimal Kitaev chain, *Phys. Rev. Appl.* **20**, 044081 (2023).
- [18] J. Wang, S. Paesani, R. Santagati, S. Knauer, A. A. Gentile, N. Wiebe, M. Petruzzella, J. L. O'Brien, J. G. Rarity, A. Laing, and M. G. Thompson, Experimental quantum Hamiltonian learning, *Nature Physics* **13**, 551 (2017).
- [19] J. R. Taylor, J. D. Sau, and S. Das Sarma, Machine learning the disorder landscape of majorana nanowires, *Phys. Rev. Lett.* **132**, 206602 (2024).
- [20] C. Bonizzoni, M. Tincani, F. Santanni, and M. Affronte, Machine-learning-assisted manipulation and readout of molecular spin qubits, *Phys. Rev. Appl.* **18**, 064074 (2022).
- [21] P. Henderson, A. Ghazaryan, A. A. Zibrov, A. F. Young, and M. Serbyn, Deep learning extraction of band structure parameters from density of states: A case study on trilayer graphene, *Phys. Rev. B* **108**, 125411 (2023).

- [22] M. Khosravian, R. Koch, and J. L. Lado, Hamiltonian learning with real-space impurity tomography in topological moiré superconductors, *Journal of Physics: Materials* **7**, 015012 (2024).
- [23] D. Liu, A. B. Watson, M. Hott, S. Carr, and M. Luskin, Learning the local density of states of a bilayer moiré material in one dimension (2025), arXiv:2405.06688 [math-ph].
- [24] Q. Gu, Z. Zhouyin, S. K. Pandey, P. Zhang, L. Zhang, and W. E, Deep learning tight-binding approach for large-scale electronic simulations at finite temperatures with ab initio accuracy, *Nature Communications* **15**, 6772 (2024).
- [25] K. Choudhary, Slakonet: A unified slater-koster tight-binding framework using neural network infrastructure for the periodic table, *The Journal of Physical Chemistry Letters* **16**, 11109 (2025).
- [26] M. Mattheakis, D. Sondak, A. S. Dogra, and P. Protopapas, Hamiltonian neural networks for solving equations of motion, *Phys. Rev. E* **105**, 065305 (2022).
- [27] S. Greydanus, M. Dzamba, and J. Yosinski, Hamiltonian neural networks, *Advances in neural information processing systems* **32** (2019).
- [28] A. Mirani and P. Hayden, Learning interacting fermionic Hamiltonians at the Heisenberg limit, *Phys. Rev. A* **110**, 062421 (2024).
- [29] D. Stilck França, L. A. Markovich, V. V. Dobrovitski, A. H. Werner, and J. Borregaard, Efficient and robust estimation of many-qubit Hamiltonians, *Nature Communications* **15**, 311 (2024).
- [30] D. Hangleiter, I. Roth, J. Fuksa, J. Eisert, and P. Roushan, Robustly learning the Hamiltonian dynamics of a superconducting quantum processor, *Nature Communications* **15**, 9595 (2024).
- [31] F. Borsoi, N. W. Hendrickx, V. John, M. Meyer, S. Motz, F. van Riggelen, A. Sammak, S. L. de Snoo, G. Scappucci, and M. Veldhorst, Shared control of a 16 semiconductor quantum dot crossbar array, *Nature Nanotechnology* **19**, 21 (2024).
- [32] A. R. Mills, D. M. Zajac, M. J. Gullans, F. J. Schupp, T. M. Hazard, and J. R. Petta, Shuttling a single charge across a one-dimensional array of silicon quantum dots, *Nature Communications* **10**, 1063 (2019).
- [33] A. Shandilya, S. Kapila, R. Krishnan, B. Weber, and B. Muralidharan, Unified simulation framework for experimentally-observed spin-valley locking in MoS₂ quantum dots: Implications for qubit applications, *ACS Applied Nano Materials* **8**, 14949 (2025).
- [34] M. Leijnse and K. Flensberg, Parity qubits and poor man's majorana bound states in double quantum dots, *Phys. Rev. B* **86**, 134528 (2012).
- [35] T. Dvir, G. Wang, N. van Loo, C.-X. Liu, G. P. Mazur, A. Bordin, S. L. D. ten Haaf, J.-Y. Wang, D. van Driel, F. Zatelli, X. Li, F. K. Malinowski, S. Gazibegovic, G. Badawy, E. P. A. M. Bakkers, M. Wimmer, and L. P. Kouwenhoven, Realization of a minimal kitaev chain in coupled quantum dots, *Nature* **614**, 445 (2023).
- [36] A. Bordin, C.-X. Liu, T. Dvir, F. Zatelli, S. L. D. ten Haaf, D. van Driel, G. Wang, N. van Loo, Y. Zhang, J. C. Wolff, T. Van Caekenberghe, G. Badawy, S. Gazibegovic, E. P. A. M. Bakkers, M. Wimmer, L. P. Kouwenhoven, and G. P. Mazur, Enhanced majorana stability in a three-site kitaev chain, *Nature Nanotechnology* **10.1038/s41565-025-01894-4** (2025).
- [37] I. C. Fulga, A. Haim, A. R. Akhmerov, and Y. Oreg, Adaptive tuning of majorana fermions in a quantum dot chain, *New Journal of Physics* **15**, 045020 (2013).
- [38] M. M. Maška and T. Domański, Polarization of the Majorana quasiparticles in the Rashba chain, *Scientific Reports* **7**, 16193 (2017).
- [39] J. Darulová, S. Pauka, N. Wiebe, K. Chan, G. Gardener, M. Manfra, M. Cassidy, and M. Troyer, Autonomous tuning and charge-state detection of gate-defined quantum dots, *Phys. Rev. Appl.* **13**, 054005 (2020).
- [40] J. P. Zwolak and J. M. Taylor, Colloquium: Advances in automation of quantum dot devices control, *Rev. Mod. Phys.* **95**, 011006 (2023).
- [41] M.-A. Roux, J. Rivard, V. Yon, A. Morel, D. Leclerc, C. Rohrbacher, E. B. Ndiaye, F. F. Tafuri, B. Bono, S. Kubicek, R. Loo, Y. Shimura, J. Jussot, C. Godfrin, D. Wan, K. D. Greve, M.-A. Tétrault, D. Drouin, C. Lupien, M. Pioro-Ladrière, and E. Dupont-Ferrier, Rapid autotuning of a sige quantum dot into the single-electron regime with machine learning and RF-reflectometry FPGA-based measurements (2025), arXiv:2509.19537 [cond-mat.mes-hall].
- [42] M. P. R. Losert, D. Denora, B. van Straaten, M. Chan, S. D. Oosterhout, L. Stehouwer, G. Scappucci, M. Veldhorst, and J. P. Zwolak, Automated electrostatic characterization of quantum dot devices in single- and bilayer heterostructures (2025), arXiv:2601.00067 [cond-mat.mes-hall].
- [43] A. Donarini and M. Grifoni, *Quantum Transport in Interacting Nanojunctions* (Springer, 2024).
- [44] G. E. Blonder, M. Tinkham, and T. M. Klapwijk, Transition from metallic to tunneling regimes in superconducting microconstrictions: Excess current, charge imbalance, and supercurrent conversion, *Phys. Rev. B* **25**, 4515 (1982).
- [45] J. R. Taylor, J. D. Sau, and S. Das Sarma, Machine learning the disorder landscape of Majorana nanowires, *Phys. Rev. Lett.* **132**, 206602 (2024).
- [46] J. R. Taylor and S. Das Sarma, Neural network based deep learning analysis of semiconductor quantum dot qubits for automated control, *Phys. Rev. B* **111**, 035301 (2025).
- [47] D. van Driel, R. Koch, V. P. M. Sietses, S. L. D. ten Haaf, C.-X. Liu, F. Zatelli, B. Roovers, A. Bordin, N. van Loo, G. Wang, J. C. Wolff, G. P. Mazur, T. Dvir, I. Kulesh, Q. Wang, A. M. Bozkurt, S. Gazibegovic, G. Badawy, E. P. A. M. Bakkers, M. Wimmer, S. Goswami, J. L. Lado, L. P. Kouwenhoven, and E. Greplova, Cross-platform autonomous control of minimal kitaev chains (2024), arXiv:2405.04596 [cond-mat.mes-hall].
- [48] J. R. Taylor and S. Das Sarma, Mitigating disorder and optimizing topological indicators with vision-transformer-based neural networks in Majorana nanowires, *Phys. Rev. B* **112**, L041110 (2025).
- [49] M. M. Bronstein, J. Bruna, T. Cohen, and P. Veličković, Geometric Deep Learning: Grids, Groups, Graphs, Geodesics, and Gauges, arXiv preprint arXiv:2104.13478 (2021).
- [50] M. Raissi, P. Perdikaris, and G. Karniadakis, Physics-informed neural networks: A deep learning framework for solving forward and inverse problems involving nonlinear partial differential equations, *Journal of Computational Physics* **378**, 686 (2019).

- [51] N. Kovachki, Z. Li, B. Liu, K. Azizzadenesheli, K. Bhattacharya, A. Stuart, and A. Anandkumar, Neural operator: learning maps between function spaces with applications to pdes, *J. Mach. Learn. Res.* **24** (2023).
- [52] Z. Li, H. Zheng, N. Kovachki, D. Jin, H. Chen, B. Liu, K. Azizzadenesheli, and A. Anandkumar, Physics-informed neural operator for learning partial differential equations, *ACM / IMS J. Data Sci.* **1**, 10.1145/3648506 (2024).
- [53] M. Krawczyk, J. Pawłowski, M. M. Maška, and K. Roszak, Data-driven criteria for quantum correlations, *Phys. Rev. A* **109**, 022405 (2024).
- [54] M. Kliczkowski, L. Keyes, S. Roy, T. Paiva, M. Randeria, N. Trivedi, and M. M. Maška, Autoencoder-based analytic continuation method for strongly correlated quantum systems, *Phys. Rev. B* **110**, 115119 (2024).
- [55] P. Leszczyński, K. Kutorasiński, M. Szewczyk, and J. Pawłowski, Machine-learned models for power magnetic material characteristics, *IEEE Transactions on Power Electronics* **40**, 1554 (2025).
- [56] M. Krawczyk and J. Pawłowski, Ai-enhanced tuning of quantum dot Hamiltonians toward majorana modes (2026), arXiv:2601.02149 [cond-mat.mes-hall].
- [57] M. Elhamod, J. Bu, C. Singh, M. Redell, A. Ghosh, V. Podolskiy, W.-C. Lee, and A. Karpatne, Cophy-pgmn: Learning physics-guided neural networks with competing loss functions for solving eigenvalue problems, *ACM Trans. Intell. Syst. Technol.* **13**, 10.1145/3530911 (2022).
- [58] H. Li, Z. Wang, N. Zou, M. Ye, R. Xu, X. Gong, W. Duan, and Y. Xu, Deep-learning density functional theory hamiltonian for efficient ab initio electronic-structure calculation, *Nature Computational Science* **2**, 367 (2022).
- [59] A. Bordin, C.-X. Liu, T. Dvir, F. Zatelli, S. L. D. ten Haaf, D. van Driel, G. Wang, N. van Loo, Y. Zhang, J. C. Wolff, T. V. Caekenberghe, G. Badawy, S. Gazibegovic, E. P. A. M. Bakkers, M. Wimmer, L. P. Kouwenhoven, and G. P. Mazur, Enhanced Majorana stability in a three-site Kitaev chain, *Nature Nanotechnology* **20**, 726 (2025).
- [60] T. Christiansen and M. Zworski, A mathematical formulation of the Mahaux–Weidenmüller formula for the scattering matrix, *Journal of Physics A: Mathematical and Theoretical* **42**, 415202 (2009).
- [61] A. Dosovitskiy, L. Beyer, A. Kolesnikov, D. Weissenborn, X. Zhai, T. Unterthiner, M. Dehghani, M. Minderer, G. Heigold, S. Gelly, J. Uszkoreit, and N. Houlsby, An image is worth 16x16 words: Transformers for image recognition at scale, in *International Conference on Learning Representations* (2021).

Supplementary Material for “Learning Hamiltonians for solid-state simulators”

Jarosław Pawłowski and Mateusz Krawczyk
*Institute of Theoretical Physics, Wrocław University of Science and Technology,
Wybrzeże Wyspiańskiego 27, 50-370 Wrocław, Poland*

CHAIN OF N RASHBA QUANTUM DOTS

Analytical considerations

We start with the Rashba-Zeeman-BCS Hamiltonian, defined in Eq. 1, written in the Nambu spinor representation $\hat{\Psi}_n = (c_{n\uparrow}, c_{n\downarrow}, c_{n\uparrow}^\dagger, c_{n\downarrow}^\dagger)^T$ giving $H^{\text{QDs}} = \frac{1}{2} \sum_{nm} \hat{\Psi}_n^\dagger H_{nm}^{\text{BdG}} \hat{\Psi}_m$, where H^{BdG} is a first-quantized Hamiltonian, also called the Bogoliubov-de Gennes (BdG) Hamiltonian. It’s explicit matrix form reads:

$$H^{\text{BdG}} = \sum_{n=1}^N \begin{pmatrix} -\mu_n + V_Z & 0 & 0 & \Delta_n \\ 0 & -\mu_n - V_Z & -\Delta_n & 0 \\ 0 & -\Delta_n & \mu_n - V_Z & 0 \\ \Delta_n & 0 & 0 & \mu_n + V_Z \end{pmatrix}_{n,n} + \sum_{n=1}^{N-1} t_n \begin{pmatrix} e^{i\lambda_n \sigma_y} & 0 \\ 0 & -e^{-i\lambda_n \sigma_y} \end{pmatrix}_{n,n+1} + \text{h.c.}, \quad (\text{S1})$$

with the onsite (dot) block $(\)_{n,n}$ and the offsite hopping (inter-dot) block $(\)_{n,n+1}$ —both represented by 4×4 matrices. In Eq. S1 we assumed $\boldsymbol{\lambda}_n \cdot \boldsymbol{\sigma} = \lambda_n \sigma_y$, which follows from choosing the Rashba vector in a form $\boldsymbol{\lambda}_n = \lambda_n [0, 1, 0]$. For a system consisting of N quantum dots, the full BdG Hamiltonian H^{BdG} is a $4N \times 4N$ matrix.

Our goal is to simulate the Kitaev chain (KC) model, i.e., to tune the H^{BdG} (parameters) to mimic KC Hamiltonian form. The first step is that each QD should have a pair of zero energy levels $E_n = 0$. Diagonalizing a (separated) single dot block $(\)_{n,n}$ yields the condition for this to happen: $V_Z = \sqrt{\Delta_n^2 + \mu_n^2}$ or equivalently $\Delta_n = \sqrt{V_Z^2 - \mu_n^2}$. When this condition is satisfied, each dot has a pair of fermionic excitations a_n, a_n^\dagger , where

$$a_n = \frac{1}{\sqrt{2V_Z}} \left(\sqrt{V_Z + \mu_n} c_{n\uparrow}^\dagger - \sqrt{V_Z - \mu_n} c_{n\downarrow} \right). \quad (\text{S2})$$

The energy of a_n (a_n^\dagger) is zero. Two other modes are separated by the energy $\pm 2V_Z$. Let’s now assume that the hopping is much smaller than the energy of the excited state, $t \ll 2V_Z$, we may project the Hamiltonian (S1) onto the Hilbert space spanned by a set $\{a_1, a_1^\dagger, a_2, a_2^\dagger, \dots, a_N, a_N^\dagger\}$. The resulting projected Hamiltonian is:

$$\tilde{H}^{\text{BdG}} = \sum_{n=1}^{N-1} \frac{t_n}{V_Z} \begin{pmatrix} -\mu_n \cos \lambda_n & \Delta_n \sin \lambda_n \\ -\Delta_n \sin \lambda_n & \mu_n \cos \lambda_n \end{pmatrix}_{n,n+1} + \text{h.c.} \quad (\text{S3})$$

The goal is to simulate the KC model, which, e.g. for $N = 2$ takes the form (in the same Nambu representation $(a_1, a_1^\dagger, a_2, a_2^\dagger)$ as \tilde{H}^{BdG}):

$$H^{\text{KC}} = \begin{pmatrix} \mu'_1 & 0 & -t'_1 & \Delta'_1 \\ 0 & -\mu'_1 & -\Delta'_1 & t'_1 \\ -t'_1 & -\Delta'_1 & \mu'_2 & 0 \\ \Delta'_1 & t'_1 & 0 & -\mu'_2 \end{pmatrix}. \quad (\text{S4})$$

KC Hamiltonian, Eq. S4, at the *sweet spot* $\mu'_n = 0$, $t'_n = \Delta'_n$ possesses two MZMs. For the Rashba-Zeeman s -wave Hamiltonian \tilde{H}^{BdG} , Eq. S3, to simulate H^{KC} , Eq. S4, at the sweet spot, the following condition must be satisfied by the Rashba length

$$\lambda_n = \arctan\left(\frac{\mu_n}{\Delta_n}\right), \quad (\text{S5})$$

which together with $\mu_n = \sqrt{V_Z^2 - \Delta_n^2}$, gives the approximate position of the parameters sweet spot for the QDs Hamiltonian H^{QDs} .

Parameters sweet spot

If we put the assumed $V_Z = 0.5$ meV and $\Delta_n = 0.25$ meV, $\sqrt{V_Z^2 - \Delta_n^2}$ gives approximately 0.43 meV, and $\arctan(\frac{\mu_n}{\Delta_n}) \simeq 0.33\pi$. However, the numerically tuned sweet spot values for $N = 3$ are slightly different: $\mu_n = 0.6$ meV and $\lambda_n = 0.27\pi$. These parameters are optimized to ensure that the formed MZMs exhibit both large edge localization and preserved particle-hole symmetry, as shown in Figs. 2(b,c) of the main text. The latter values are selected as the reference parameters, P_0 in the main text.

CONDUCTANCE NOISE MODELS

The synthetic conductance maps $G_{ij}(E_F, \Delta l)$ were augmented with two dominant noise contributions according to

$$\tilde{G}_{ij}(E_F, \Delta l) = G_{ij}^{\text{warp}}(E_F, \Delta l) + \delta G_{ij}^{\text{add}}(E_F, \Delta l), \quad (\text{S6})$$

where E_F is the Fermi energy in the leads and l denotes the detuned control parameter.

The warping contribution was implemented as a stochastic deformation of the detuning axis,

$$G_{ij}^{\text{warp}}(E_F, \Delta l) = G_{ij}(E_F, \Delta l + \delta l(E_F)), \quad (\text{S7})$$

where $\delta l(E_F)$ represents a random shift of the effective detuning value for each scan line at fixed E_F (G map is composed of 100 lines). This shift was composed of a smooth drift component $\delta l_d(E_F)$ and a random telegraph component $\delta l_t(E_F)$:

$$\delta l(E_F) = \delta l_d(E_F) + \delta l_t(E_F). \quad (\text{S8})$$

The smooth drift component was generated as a low-frequency random process along the scan direction,

$$\delta l_d(E_F) = \sigma_d f(E_F), \quad (\text{S9})$$

where $f(E_F)$ is a zero-mean Gaussian random function smoothed along the E_F axis, with a correlation length of 5-30 scan lines, meaning that significant changes of $\delta l_d(E_F)$ occur only after several consecutive lines rather than between neighboring conductance pixels; and σ_d controls the drift amplitude (randomly sampled between 0.2% and 2% of the detuning range).

The random telegraph component was defined as a piecewise-constant process,

$$\delta l_t(E_F) = \sum_{n=1}^{N_j} A_n \Theta(E_F - E_n), \quad (\text{S10})$$

where N_j is the number of telegraph jumps (randomly sampled between 0 and 3), E_n are randomly chosen scan-line positions, A_n are jump amplitudes uniformly sampled between 0.5% and 5% of the detuning range, and Θ denotes the Heaviside step function. Each term produces a sudden shift of conductance features for all subsequent scan lines.

The additive noise contribution was defined as

$$\delta G_{ij}^{\text{add}}(E_F, \Delta l) = \eta_w(E_F, \Delta l) + \eta_c(E_F, \Delta l), \quad (\text{S11})$$

where $\eta_w(E_F, \Delta l)$ is an uncorrelated Gaussian white noise and $\eta_c(E_F, \Delta l)$ is a Gaussian noise correlated along the scan direction. The standard deviation of η_w was randomly sampled between 0.5% and 3% of the maximal conductance value G_{max} . The correlated component η_c had correlation length between 2 and 10 scan lines and amplitude between 0.2% and 2% of G_{max} . During training, all noise parameters were randomly sampled within these ranges.